Nat. Hazards Earth Syst. Sci., 12, 3139–3150, 2012
www.nat-hazards-earth-syst-sci.net/12/3139/2012/
doi:10.5194/nhess-12-3139-2012

Natural Hazards and Earth System Sciences

Assessment of remotely sensed drought features in vulnerable agriculture

N. R. Dalezios[1,*], **A. Blanta**[1], **and N. V. Spyropoulos**[2]

[1]Laboratory of Agrometeorology, Department of Agriculture, Ichthyology & Aquatic Environment, School of Agricultural Sciences, University of Thessaly, Volos, Greece
[2]Department of Natural Resources Development and Agricultural Engineering, Agricultural University of Athens, Athens, Greece
[*]currently at: Senior Research Associate, Institute of Technology & Management of Agricultural Ecosystems (ITEMA)/Center for Research and Technology, Thessaly (CE.RE.TE.TH), First Industrial Area, Volos, Greece

Correspondence to: N. R. Dalezios (dalezios.n.r@gmail.com)

Received: 17 May 2012 – Revised: 3 July 2012 – Accepted: 5 July 2012 – Published: 19 October 2012

Abstract. The growing number and effectiveness of Earth observation satellite systems, along with the increasing reliability of remote sensing methodologies and techniques, present a wide range of new capabilities in monitoring and assessing droughts. A number of drought indices have been developed based on NOAA-AVHRR data exploiting the remote sensing potential at different temporal scales. In this paper, the remotely sensed Reconnaissance Drought Index (RDI) is employed for the quantification of drought. RDI enables the assessment of hydro-meteorological drought, since it uses hydrometeorological parameters, such as precipitation and potential evapotranspiration. The study area is Thessaly, central Greece, which is a drought-prone agricultural region characterized by vulnerable agriculture. Several drought features are analyzed and assessed by using monthly RDI images over the period 1981–2001: severity, areal extent, duration, periodicity, onset and end time. The results show an increase in the areal extent during each drought episode and that droughts are classified into two classes, namely small areal extent drought and large areal extent drought, respectively, lasting 12 or 13 months coinciding closely with the hydrological year. The onset of large droughts coincides with the beginning of the hydrological year, whereas the onset of small droughts is in spring. During each drought episode, the maximum occurs usually in the summer and they all last until the end of the hydrological year. This finding could justify an empirical prognostic potential of drought assessment.

1 Introduction

Drought is a natural phenomenon that has been recurring at a regional scale throughout history. Drought is also considered as one of the major natural hazards with significant impact to environment, society, agriculture and economy. Moreover, drought is referred to as "non-event", since its basic cause is the lack of precipitation events in a region over a period of time and can be regarded as an extreme climatic phenomenon associated with water resources deficit. Droughts occur in both high and low rainfall areas and virtually all climate regimes. Drought impacts are very critical and especially costly affecting more people than any other type of natural disaster universally (Kyeantash and Dracup, 2002). It is difficult to determine the effects of drought as it constitutes a complicated phenomenon, evolving gradually in any single region.

The identification and quantification of drought is not an easy task. It is recognized that there is no universally accepted definition of drought, because there is a wide variety of sectors affected by drought, its diverse spatial and temporal distribution and the demand placed on water supply by human-used systems (Heim, 2002). Drought indicators are variables that describe features of drought (Steinemann et al., 2005). Several indicators can also be synthesized into a single indicator on a quantitative scale, called a drought index. In fact, the monitoring and assessment of drought conditions in a region is usually performed through drought indices (Anderson et al., 2011; Ashok et al., 2011).

In evaluating the overall utility of indices, a set of weighted decision criteria is assigned to each index, which are based on desirable properties of each index: robustness, tractability, transparency, sophistication, expendability and dimensionality (Keyantash and Dracup, 2002). It is clear that the above criteria weights, which reflect the relative importance of the evaluation criteria, are difficult to be precisely justified. The list may be expanded or condensed, but the above criteria provide a reasonable framework for the evaluation of drought indices without excessive complication.

There are several drought indices based on ground (conventional) and/or remotely sensed data (Kanellou et al., 2011). Satellite images and data are consistently available and can be used to detect several features. Remote sensing has gradually become an important tool for the detection of the spatial and temporal distribution and characteristics of drought at different scales (Caccamo et al., 2011; Huang et al., 2011). On the other hand, drought quantification methods rely on conventional hydrometeorological data, which are usually limited in a region, often inaccurate and most significant unavailable in near real-time (Thenkabail et al., 2004). At the present time, the growing number and effectiveness of pertinent Earth observation satellite systems present a wide range of new capabilities, which can be used to assess and monitor the effects of drought. Moreover, in order to assess and monitor the drought phenomenon and to alleviate the impacts of droughts, it is necessary to detect several drought features such as severity, duration, periodicity, areal extent, onset and end time and to link drought variability to climate and its variability (Dalezios et al., 2000; Piechota and Dracup, 1996). Thus, it is clear that there is a need for proper quantification of drought impacts and monitoring of drought development is of critical importance in economically and environmentally sensitive regions. Both are very significant inputs in any drought preparedness and mitigation plan.

The objective of this paper consists of exploring the remote sensing potential in terms of data and methods in order to quantify drought and assess several drought features and characteristics. In this paper, the Reconnaissance Drought Index (RDI) is used, which is a new index suitable for hydrometeorological drought estimation (Tsakiris and Vangelis, 2005). RDI is properly adjusted to incorporate satellite data. The paper is organized as follows: in Sect. 2 drought types and remote sensing are explained. In Sect. 3 the study area is described. In Sect. 4 the remotely sensed methodology for RDI estimation is presented along with database, and several drought features are described and estimated as well as the evaluation procedure. Finally, in Sect. 5 results are analyzed and discussed.

2 Drought types and remote sensing

If drought is considered as a phenomenon, it is certainly an atmospheric phenomenon. Specifically, droughts have been shown to be associated with the persistence of ridges or centers of high pressure systems at middle level in the troposphere. Furthermore, the corresponding reduced cloud cover results in positive temperature anomalies in the lower atmosphere, which produces the middle-level pressure anomaly and favours subsidence at the high level keeping the atmosphere significantly drier and more stable than normal (Dalezios et al., 2009). Studies in several parts of the world have shown that drought periods are often characterized by large decrease in the amount of rainfall per day, by an increase in the continentality of the clouds and a lack of rain-producing clouds.

Usually, drought is considered as a hazard, and there is a tendency to classify drought types into three categories: meteorological or climatological, agrometeorological or agricultural and hydrological drought, including as a fourth class the socioeconomic impacts (Keyantash and Dracup, 2002). A brief description follows.

- Meteorological or climatological drought is generally characterized by a precipitation anomaly being lower than average in a region for some period of time and by prolonged and abnormal moisture deficiency.

- Agrometeorological or agricultural drought is described in terms of crop failure and exists when soil moisture is depleted so that crop yield is reduced considerably.

- Hydrological drought is considered to be a period during which the actual water supply, either surface water or groundwater, is less than the minimum water supply necessary for normal operations in a particular region (watershed).

- Socioeconomic impacts of drought are defined in terms of loss from an average or expected return and can be measured by both social and economic indicators (McVicar and Jupp, 1998).

The relationship between the different drought types is complex. For example, streamflow is the key variable for many water supply activities in a semi-arid region, such as hydropower generation, recreation and irrigated agriculture, where crop growth and yield are largely dependent on water availability (Heim, 2002). A single unifying technique is not usually sufficient to quantify drought severity. Even within an individual category, the supremacy of a specific index is not immediately clear.

The application and utility of remote sensing to drought assessment is growing rapidly, mainly due to the increasing number of pertinent satellite systems and their capabilities and impacts to climatic variability and/or change. Remote sensing methodologies and techniques can be employed in several aspects of drought, such as vulnerability and damage assessment and warning (Du et al., 2012; Rhee at al., 2010). The possible contribution of remote sensing could

Table 1. Satellite-based drought indices and corresponding drought type.

Index	Type of drought
1. Normalized Difference Vegetation Index (NDVI)	Agricultural
2. Deviation $_{NDVI}$ Index	Agricultural
3. Enhanced Vegetation Index (EVI)	Agricultural
4. Vegetation Condition Index (VCI)	Agricultural
5. Monthly Vegetation Condition Index	Agricultural
6. Temperature Condition Index (TCI)	Agricultural
7. Vegetation Health Index (VHI)	Agricultural
8. Normalised Difference Temperature Index (NDTI)	Agricultural
9. Crop Water Stress Index (SWSI)	Hydrological
10. Drought Severity Index (DSI)	Hydrological
11. Temperature-Vegetation Dryness Index (TVDI)	Agricultural
12. Normalized Difference Water Index (NDWI)	Hydrological
13. Reconnaissance Drought Index (RDI)	Hydrological

be focused on relief and, possibly, preparedness or warning (Williams, 1993; Foot, 1993), although in many cases remote sensing can make a valuable contribution to disaster prevention, where frequency of observation is not such a prohibitive limitation.

A major consideration for development of remote sensing for drought assessment and disaster reduction is the extent to which operational users can rely on a continued supply of data (Colwell, 1984). In this context there are two types of remote sensing systems for drought assessment: meteorological and environmental (or resource) satellites. Meteorological satellites have also two types, namely geostationary such as METEOSAT and geosynchronous such as NOAA/AVHRR, and can contribute to operational monitoring and assessment of drought (Caccamo et al., 2011; Zhou et al., 2012). Similarly, environmental satellites such as LANDSAT, SPOT and recently IKONOS, WV2 with high to very high resolution, but low frequency of coverage, can contribute to land-use classification and qualitative features of drought and less to quantitative assessments (Peled et al., 2010). Table 1 presents an indicative list of internationally used remotely sensed drought indices. There is also a larger list of conventional drought indices (Kanellou et al., 2011), where most of them can be adjusted to incorporate remotely sensed data.

In this paper, the Reconnaissance Drought Index (RDI) is used for the quantification of drought based on remote sensing. RDI is a new index, which is used for hydrometeorological drought estimation (Tsakiris and Vangelis, 2005; Tsakiris et al., 2007). RDI is a physically based and general index and can be used in a variety of climatic conditions. Moreover, RDI provides information for the water deficit in an area as it is based not only on precipitation, but also on potential evapotranspiration. In order to assess and monitor drought, it is also necessary to detect several drought features. In fact, remote sensing data and methods can delineate the spatial and temporal variability of several drought features in quantitative terms.

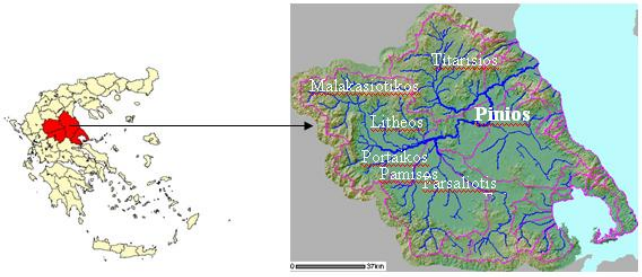

Fig. 1. Geophysical map of Thessaly region.

3 Study area

Thessaly is one of the thirteen hydrological districts of Greece located in the central part of the country. Thessaly has a total area of 14.036 km^2, which roughly represents 10.6 % of the whole country. Moreover, in Thessaly 36 % of the land is flat, 17.1 % is semi-mountainous, whereas the remaining 44.9 % is mountainous. The region of Thessaly is characterized by a highly variable landscape, and the terrain is such that high mountains surround the plain, which is the largest in the country (Fig. 1).

The plain of Thessaly is crossed by Pinios River. Thessaly water district is divided into three watersheds, where the main one is the Pinios basin with 9500 km^2 in size, Lake Karla basin with 1050 km^2 in size, and the remaining basins and subbasins cover an area of 2827 km^2. Pinios River after the mountainous terrain crosses the alluvial basin of the Thessaly plain, which is then divided into two parts, with the main tributaries being Titarisios, Enipeas, Kalentzis and Litheos. The main part of the Pinios watershed includes a mountainous terrain with altitudes higher than 2000 m, as in Olympus (north) and Pindos (west), agricultural plains (the Thessaly plain) and urban areas with mean elevation of 285 m. The alluvial plain of Pinios River is a sensitive and complex hydrogeological environment. Surface and groundwater resources are jointly used to cover rural, urban and industrial water needs, as well as preservation of wetland in the region. Impermeable geological structures cover 30.6 % of the total area, karstic aquifers 14.5 % and permeable structures, which occur mainly on the plain, cover 42.7 %.

The climate of Thessaly is continental in the west part with cold winters, hot summers and large seasonal temperature range. In the east part of Thessaly, the climate is typical Mediterranean. In Thessaly, summers are usually hot and dry with temperatures occasionally reaching 40 °C in July and August. Mean annual precipitation over Thessaly is about 700 mm, unevenly distributed in space and time, varying from about 400 mm at the central plain to more than 1850 mm at the western mountain peaks. The mountain areas receive significant amounts of snow during winter months. At the Thessaly plain, around Larissa and Karla basin, the mean annual precipitation ranges between 250 and 500 mm,

having reduced over the last 30 years about 20 %. Moreover, since rainfall is, in general, rare from June to August, the resulted water deficit is replaced by irrigation in order to satisfy agricultural water needs.

The Thessaly plain constitutes the main agricultural area of the country, with cotton being still the major crop; however, wheat, sugar beets, maize, barley, horticulture, fruits, olive trees and recently energy crops are also cultivated in the region. At the present time, in practical terms, the annual water availability is about 1023 million m^3, consisting of surface (623 million m^3) and groundwater (400 million m^3), whereas the annual water needs amount to 1836 million m^3. There is, thus, an annual water deficit of 813 million m^3. Part of it (about 600 million m^3) is expected to be covered from Acheloos dam. Moreover, the amount of water used for irrigation purposes accounts for about 96 % and the remaining about 3.3 % of the total water consumption is used for other water needs in the catchment. Furthermore, the irrigated areas have significantly increased over the last decades reaching about 252 500 ha in recent years. The irrigated areas are expected to further increase in Thessaly. Thus, the future water needs are also expected to increase despite scheduled crop restructuring programs.

Thessaly is characterized by vulnerable agriculture, since extreme hydrometeorological events such as floods, hail and droughts are quite common in the catchment, but also due to the existing water deficit for agriculture. Thessaly is considered as one of the most important agricultural regions in the country, and drought episodes could have enormous environmental and socioeconomic impacts. Droughts occur mainly due to reduced precipitation causing lack of soil moisture, increased evapotranspiration, runoff reduction, decrease in streamflow levels in rivers, lakes and dams, lowering of the groundwater table, thus resulting in water deficit for agriculture. Drought is the subject of this paper and several drought features are explored through remote sensing and analysed and presented in subsequent sections.

4 Methodology

The methodology includes drought quantification by the use of RDI, extraction and computation of several drought features, as well as evaluation. The estimation of RDI is based on remote sensing data and techniques. In the computation of RDI, the innovation consists of employing Blaney-Criddle method for potential evapotranspiration instead of Thornthwaite method, since it is more appropriate for the Mediterranean region with dry and hot summers (Blaney and Criddle, 1950). Furthermore, in this paper Blaney-Criddle method is based on land surface temperature (LST), which is derived from satellite data (Kanellou et al., 2009).

4.1 Remotely sensed estimation of RDI

The estimation of RDI from remotely sensed data on a monthly and annual basis follows certain steps. At first, preprocessing of satellite images is implemented, which includes geometric and atmospheric correction of all images. Then, from 10-day BT and NDVI images, on a pixel basis, land surface temperature (LST) images are produced, which then through regression analysis lead to air temperature (Tair) estimation on a pixel basis. The next step consists of the estimation of potential evapotranspiration on a pixel basis again using Blaney-Griddle method and satellite-derived Tair. Then rainfall maps are used as provided by JRC, Ispra. Finally, all the above are incorporated into the model to produce RDI estimates on a pixel basis. A brief description follows.

4.1.1 Calculation of air temperature

The procedure for the extraction of LST includes the use of the following empirical Eq. (1) (Kanellou et al., 2011):

$$T = (\text{image pixel} + 31\,990) * 0.005, \quad (1)$$

where image pixel is the pixel value from the thermal band and T is temperature in kelvin (K), which is then converted to values of degrees celsius (°C). For the elimination of the water vapour effect in infra-red radiation and the transmitted radiation from the surface, the algorithm of "split window" (Becker and Li, 1990) is employed. This method achieves atmospheric correction of the satellite data including water vapour absorption. The equation of Becker and Li is given by Eq. (2):

$$\begin{aligned} T = {} & 1.274 + (T_4 + T_5)/2[1 + 0.15616\{(1-e)/e\} \\ & - 0.482 de/e * *2] + (T_4 - T_5)/2[6.26 + 3.989\{(1-e)/e\} \\ & + 38.33 de/e * *2] \end{aligned} \quad (2)$$

where T is the land surface temperature (LST) in °C, and T_4 and T_5 are the values of thermal bands 4 and 5 of the satellite, respectively. The variables e and de of Eq. (2) are defined by

$$e = (e_4 + e_5)/2 \quad (3)$$

$$de = e_4 - e_5 \quad (4)$$

where e_4 and e_5 are the reflection values of bands 4 and 5, respectively, which estimate the transmission of infrared radiation from the surface and are given by Van de Griend and Owe (1993) empirical equations:

$$e_4 = 1.0094 + 0.047 \ln(\text{NDVI}) \quad (5)$$

$$e_5 = e_4 + 0.01 \quad (6)$$

where NDVI is the values of the index.

A regression analysis is conducted between the derived monthly LST values from Eq. (2) and the corresponding

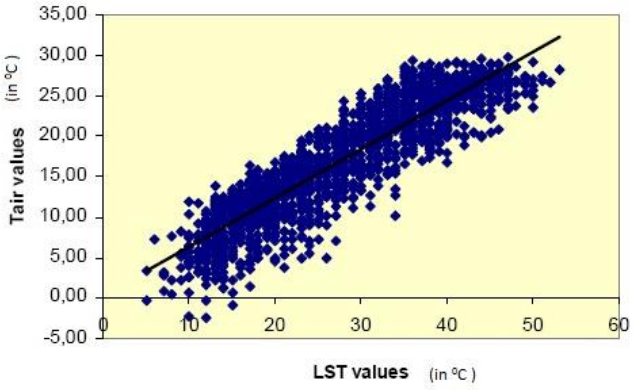

Fig. 2. LST and air temperature (Tair) for Larissa (°C).

monthly air temperature (Tair) values from Larissa station for the 20-yr period (1981–2001). The resulting empirical Eq. (7) is given below, along with the plotted values (Fig. 2). Finally, from Eq. (7) monthly air temperature maps (images) of Thessaly are produced on a pixel basis.

$$T_{\text{air}} = 0.6143 - \text{LST} + 7.3674 \quad R^2 \approx 0.82 \tag{7}$$

4.1.2 Estimation of potential evapotranspiration

In this paper potential evapotranspiration is estimated with the use of Blaney-Criddle method, which has been originally applied in California. This method is selected in this paper, since it is appropriate for subtropical climates with dry and hot summers such as Mediterranean region. Blaney and Criddle (1950) method estimates the potential evapotranspiration (PET_k) for the month k in mm, through Eq. (8):

$$\text{PET}_k = k_c * [0.46T + 8.16] * p \tag{8}$$

where T is the mean monthly air temperature for month k, p is the monthly daytime sunshine duration, which depends on the latitude of the area, and k_c is the crop coefficient, different for each cultivation, vegetation type and land use. Maps of mean monthly crop coefficients for each vegetation type and land use in $500 \times 500\,\text{m}^2$ pixel size, as well as maps of daytime sunshine duration (p) for each monthly value for the Thessaly water district (39.39° N) are extracted in a GIS environment (Kanellou et al., 2009). The monthly crop coefficient and the maps of daytime sunshine duration are combined with the air temperature maps for the whole data set in order to extract Blaney-Criddle potential evapotranspiration for each month in the time series (1981–2001).

4.1.3 Rainfall mapping

Rainfall maps over Thessaly on a monthly basis are produced. The initial data are daily rainfall measurements from numerous stations all over Europe provided by JRC, ISPRA for the period 1975–2005. Cumulative monthly rainfall values are computed per station. Then rainfall maps of $50 \times 50\,\text{km}^2$ grids are produced per region using linear interpolation techniques. In this way monthly rainfall maps are extracted for the region of Thessaly.

4.1.4 RDI estimation

The calculation of RDI starts with the estimation of a_k coefficient (Tsakiris et al., 2007), as it is given by the equation:

$$a_k = \frac{\sum_{j=1}^{j=k} P_j}{\sum_{j=1}^{j=k} \text{PET}_j} \tag{9}$$

where P_j and PET_j are the precipitation and potential evapotranspiration, respectively, of the j-th month of the hydrological year. The hydrological year for the Mediterranean region starts in October; hence, for October $k = l$. Monthly rainfall maps (P_j) of Thessaly are used as described above (Sect. 4.1.3). Similarly, monthly potential evapotranspiration maps (PET_j) of Thessaly are used based on monthly temperature maps, crop coefficient (k_c) maps, daytime sunshine duration maps (p) as explained above (Sect. 4.1.2). The normalized RDIn is given by

$$\text{RDI}_n(k) = \frac{a_k}{\overline{a_k}} - 1 \tag{10}$$

The standardized RDI (RDI_{st}), which is used in this study, is given by

$$\text{RDI}_{\text{st}}(k) = \frac{y_k - \overline{y_k}}{\hat{\sigma_k}} \tag{11}$$

where y_k is the $\ln a_k$, $\overline{y_k}$ is its arithmetic mean and $\hat{\sigma_k}$ is its standard deviation.

The drought classes based on RDI are shown in Table 2, along with the corresponding drought class number.

4.2 Database

For the RDI estimation the following data is utilized:

- daily precipitation of Thessaly water district in $50 \times 50\,\text{km}^2$ spatial analysis derived by ground measurements provided by the Joint Research Center (JRC) of EC, Ispra, Italy.
- crop coefficients maps extracted by Corine Hellas 2000 for each month of the year (12 maps).
- monthly maps of daytime sunshine duration for 39.39° N of Thessaly (12 maps).

Table 2. Drought classes based on RDI (Tsakiris and Vangelis, 2005).

RDI Classes	RDI Class Number	RDI Values
Extremely Wet		> 2.00
Very Wet		1.50 to 1.99
Moderately Wet		1.00 to 1.49
Near Normal (mild drought)	1	−0.99 to 0.99
Moderate Drought	2	−1.00 to −1.49
Severe Drought	3	−1.50 −1.99
Extreme Drought	4	< −2.00

– a time series of 10-day brightness temperature (BT) images extracted from Channels 4 and 5 for 20 consecutive hydrological years (October 1981–September 2001) $8 \times 8\,\mathrm{km}^2$ provided by NOAA.

– a time series of 10-day normalized difference vegetation index (NDVI) extracted from Channels 1 and 2 for 20 consecutive hydrological years (October 1981–September 2001) $8 \times 8\,\mathrm{km}^2$ provided by NOAA.

4.3 Drought features

As already mentioned, in order to assess and monitor drought, it is necessary to detect several drought features. Moreover, remote sensing data and methods can delineate the spatial and temporal variability of several drought features in quantitative terms. A description of some key features follows (Palmer, 1965; Kanellou et al., 2011).

Severity: severity or intensity of drought is defined as escalation of the phenomenon into classes from mild, moderate, severe and extreme. The severity is usually determined through drought indicators and indices, which include the above-mentioned classes. In the RDI estimation of severity, the above four classes are used (Table 2).

Duration: duration of a drought episode is defined as the time interval from the start and end time, usually in months. Drought duration using RDI is estimated by counting the number of successive months with negative pixel values for all the above-described severity classes.

Onset: the beginning of drought is determined by the occurrence of a drought episode. The beginning of a drought is assessed through indicators or indices reaching certain threshold value. The onset of drought using RDI coincides with the first negative pixel value.

End time: end time of a drought episode signifies the termination of drought based again on threshold values of indicators or indices. The end time of drought using RDI coincides with the last negative pixel value in successive monthly RDI values.

Areal extent: areal extent of drought is considered the spatial coverage of the phenomenon as is quantified in classes by indicators or indices. Areal extent varies in time and remote sensing has contributed significantly in the delineation of this parameter by counting the number of pixels in each class, which is followed in the present study using RDI.

Periodicity: Periodicity is considered the recurrence interval of drought. In this paper, periodicity analysis of the monthly Z-index values of Palmer (Palmer, 1965) at all stations in Thessaly is implemented by power spectrum analysis (Loukas et al., 2002). The power spectra are obtained by applying the discrete Fourier transform algorithm to the correlation functions derived from the time series (Jenkins and Watts, 1968) taking as smoothing function a classical Hamming window (Percival and Walden, 1993). In this paper, it is assumed that the time series could be derived by an autoregressive process of order one (Markov red-noise process as the null hypothesis) and the significance of the periodicities was tested at the 1 % level.

4.4 Evaluation

The accuracy of the remotely sensed estimated monthly RDI series should be assessed and evaluated. The evaluation is based on the comparison between the remotely sensed and the corresponding ground-truth RDI estimations at Larissa station for the period 1981–2001 through several error statistics. The rationale of using several statistics as possible indicators of the magnitude of errors in drought analysis and estimation comes from the fact that there is no generally accepted "best" statistics to describe the errors. In this study, four well-known and widely used error statistics are employed: the efficiency coefficient (Nash and Sutcliffe, 1970), the coefficient of determination, the statistical bias and the root-mean-square error (Dalezios, 1988). A brief description follows.

1. Efficiency coefficient (Nash and Sutcliffe, 1970)

$$\mathrm{Eff} = 1 - \frac{\sum_{i=1}^{n} \left(\mathrm{RDI}_{\mathrm{ground}} - \mathrm{RDI}_{\mathrm{satellite}}\right)^2}{\sum_{i=1}^{n} \left(\mathrm{RDI}_{\mathrm{ground}} - \overline{\mathrm{RDI}_{\mathrm{ground}}}\right)^2} \qquad (12)$$

where $\mathrm{RDI}_{\mathrm{ground}}$ are ground-based values of RDI, $\mathrm{RDI}_{\mathrm{satellite}}$ are satellite-based values of RDI, $\overline{\mathrm{RDI}_{\mathrm{ground}}}$ are mean ground-based values of RDI, n is the number of cases, i.e. monthly values for 20 yr (1981–2001). The efficiency coefficient ranges between one and $-\infty$ and for a perfect technique should be equal to one (Table 3).

Table 3. The results of error statistics (monthly RDI).

Error statistics	Estimated values	Range of fit	Perfect fit
EFF	0.7	1 to $-\infty$	1
R^2	0.87	0 to 1	1
BIAS	−0.15	≈ 0	0
RMSE from conventional data	0.98	≈ 0	0
RMSE from satellite data	0.95		0

2. Coefficient of determination (R^2)

$$R^2 = \left(\frac{\sum_{i=1}^{n} \left(\mathrm{RDI}_{\mathrm{ground}} - \overline{\mathrm{RDI}_{\mathrm{ground}}}\right)\left(\mathrm{RDI}_{\mathrm{satellite}} - \overline{\mathrm{RDI}_{\mathrm{satellite}}}\right)}{\sqrt{\sum_{i=1}^{n} \left(\mathrm{RDI}_{\mathrm{ground}} - \overline{\mathrm{RDI}_{\mathrm{ground}}}\right)^2} \sqrt{\sum_{i=1}^{n} \left(\mathrm{RDI}_{\mathrm{satellite}} - \overline{\mathrm{RDI}_{\mathrm{satellite}}}\right)^2}} \right)^2 \quad (13)$$

where $\mathrm{RDI}_{\mathrm{ground}}$ are ground-based values of RDI, $\mathrm{RDI}_{\mathrm{satellite}}$ are satellite-based values of RDI , $\overline{\mathrm{RDI}_{\mathrm{ground}}}$ are mean ground-based values of RDI, $\overline{\mathrm{RDI}_{\mathrm{satellite}}}$ are mean satellite-based values of RDI, and n is the number of cases, i.e. monthly values for 20 yr (1981–2001). The coefficient of determination ranges between zero and one, and for a perfect technique should be equal to one (Table 3).

3. Statistical bias (BIAS) (Dalezios, 1988)

$$\mathrm{BIAS} = \frac{1}{N} \sum_{i=1}^{n} \left(\mathrm{RDI}_{\mathrm{ground}} - \mathrm{RDI}_{\mathrm{satellite}}\right) \quad (14)$$

where $\mathrm{RDI}_{\mathrm{ground}}$ are ground-based values of RDI, $\mathrm{RDI}_{\mathrm{satellite}}$ are satellite-based values of RDI, and n is the number of cases. For a perfect technique, the statistical bias should be equal to zero (Table 3).

4. Root-mean-square error (RMSE) (Dalezios, 1988)

$$\mathrm{RMSE} = \sqrt{\frac{\sum_{i=1}^{n} \left(\mathrm{RDI}_{\mathrm{ground}} - \overline{\mathrm{RDI}_{\mathrm{ground}}}\right)^2}{n}} \quad (15)$$

where $\mathrm{RDI}_{\mathrm{ground}}$ are ground-based values of RDI, $\overline{\mathrm{RDI}_{\mathrm{ground}}}$ are mean ground-based values of RDI and n is the number of cases. For a perfect technique the root-mean-square error should be equal to zero (Table 3).

5 Results and discussion

The results include quantification of drought through RDI estimation on a monthly and annual basis for a period of 20 yr (1981–2001) using conventional and satellite data. The analysis of results also involves evaluation and validation of the remotely sensed drought estimation, as well as extraction of several features from drought episodes, which lead to useful inferences. The results are presented in Tables 3 to 7 and Figs. 3 to 6.

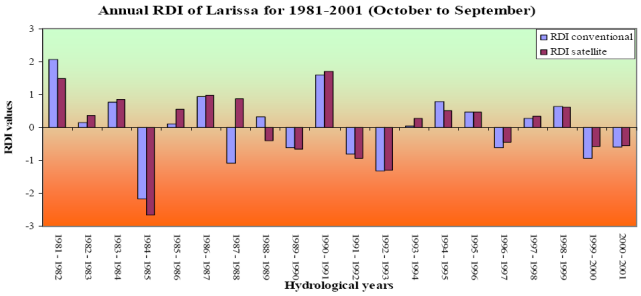

Fig. 3. Annual (October to September) RDI of Larissa for 1981–2001.

Figure 3 delineates the time series of annual RDI for Larissa (1981–2001) estimated from both conventional and remotely sensed data. This Fig. 3 initially shows that both estimation methods are in good agreement. Validation of the remotely sensed RDI estimation is attempted through the computation of several widely used error statistics: the efficiency coefficient (EFF), the coefficient of determination (R^2), the statistical bias (BIAS) and the root-mean-square error (RMSE). The results are presented in Table 3 and are considered quite satisfactory being close to the perfect values for all the four error statistics. It should be mentioned that the better a technique is, the closer the value of each error statistic to the perfect fit value. Specifically, the efficiency coefficient is 0.7, which is close to the perfect fit value of one. Similarly, the coefficient of determination is 0.87, which is also very close to the perfect fit value of one. Moreover, the statistical bias is −0.15, which is equally very close to the perfect fit value of one. Finally, the root-mean-square error is 0.98 for conventional data and 0.95 for satellite data, respectively, which are again close to the perfect fit value of zero.

Periodicity analysis has been conducted for Greece in a previous study (Loukas et al., 2002) based on power spectrum analysis of Z-index from Palmer's method (Palmer, 1965), where the statistical significance of the periodicities is tested at 1 % level. Table 4 presents the results of periodicity analysis, which is referred to stations in Thessaly, namely Larissa, Volos and Trikala, respectively. The results of Table 4 are in months and indicate short periodicity cycles ranging from two to eight months for the central part of Thessaly (Larissa station) and medium-long to long cycles ranging from 20 to 38 months and longer for coastal (Volos station) and mountainous (Trikala station) parts of Thessaly, respectively.

In these 20-yr time series of annual RDI, eight drought episodes are identified (Fig. 3). Analysis of the monthly RDI maps specifies the onset, the end time and the duration of

Table 4. Drought periodicities using the Z-index.

Station	L = Long cycles (> 38 months)	ML = Medium-Long cycles (20–38 months)	M = Medium cycles (9–19 months)	S = Short cycles (2–8 months)
Larissa			14.6	7.3, 3.1, 2.8
Volos		37.3, 25.8		3.1, 2.8
Trikala	108	25.8, 22.4		6.1

Table 5. Duration of drought episodes (in months in Thessaly).

Drought Years	Start	End	Duration
Oct 1984–Oct 1985	Oct 1984	Oct 1985	13
Oct 1987–Oct 1988	Oct 1987	Oct 1988	13
Sep 1989–Oct 1990	Sep 1989	Oct 1990	13
Oct 1991–Sep 1992	Oct 1991	Sep 1992	12
Oct 1992–Oct 1993	Oct 1992	Oct 1993	13
Oct 1996–Sep 1997	Oct 1996	Sep 1997	12
Oct 1999–Sep 2000	Oct 1999	Sep 2000	12
Oct 2000–Sep 2001	Oct 2000	Sep 2001	12

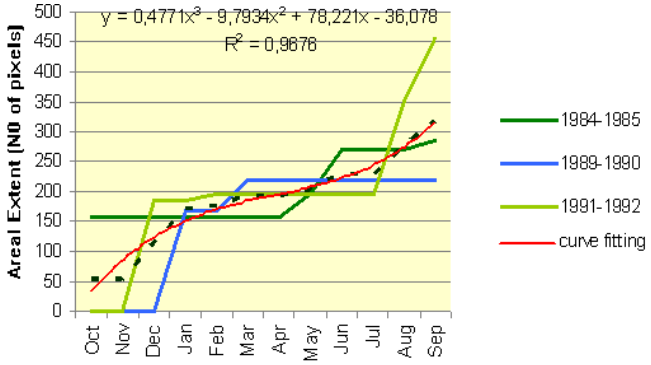

Fig. 4. Cumulative large areal extent (number of pixels 8X8 km^2) of extreme drought (>2.0) during drought years based on remotely sensed RDI.

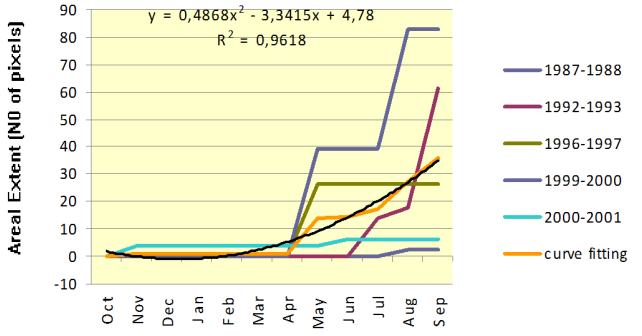

Fig. 5. Cumulative small areal extent (number of pixels 8X8 km2) of extreme drought (>2.0) during drought years based on remotely sensed RDI.

each drought episode in Thessaly as summarized in Table 5. This Table 5 shows that the duration of each episode varies between 12 and 13 months coinciding with the corresponding hydrological years. In particular, Table 5 presents the drought periods, their duration along with the start and end times based on RDI monthly estimates.

Further analysis of the monthly remotely sensed RDI images of Thessaly of the eight drought years leads to Tables 6 and 7. These Tables 6 and 7 present the monthly drought areal extent in terms of number of pixels for each of the four drought severity classes (Table 2), as well as the total for all the classes and for each month. These Tables 6 and 7 show that the majority of pixels are accumulated between mild to moderate drought severity classes indicating a significant decrease in the number of pixels from mild to extreme drought classes for all the months. Similarly, from Tables 6 and 7, it is noticed that the total areal extent in Thessaly for all the drought years ranges within the same order of magnitude.

From these Tables 6 and 7, several comments can be made about drought spatiotemporal behaviour. In particular, the cumulative monthly areal extent (Table 2) for all the drought severity classes shows the same slightly increasing trend from mild class to extreme class for all the drought years. From Tables 6 and 7, it is also shown that there is no significant increase in the areal extent from mild class to extreme class, since, as already mentioned, most of the pixels are accumulated between mild to moderate severity classes. Similarly, from Tables 6 and 7 the cumulative monthly areal extent for all the drought hydrological years shows the same increasing trend throughout each hydrological year for all drought years. Specifically, Tables 6 and 7 indicate also that there are drought years with very small areal extent at the beginning of the hydrological year reaching smaller total areal extent at the end of the hydrological year than other drought years with larger areal extent at the beginning reaching equally larger total areal extent at the end of the hydrological year.

If only the extreme drought class (class 4) of Tables 6 and 7 is considered, it can be assessed that the eight drought episodes can be classified based on areal extent and severity in two major classes: large areal extent drought with three cases (1984–1985, 1989–1990, 1991–1992) and small areal extent drought with five cases (1987–1988, 1992–1993, 1996–1997, 1999–2000, 2000–2001). By plotting the cumulative monthly areal extent values of the extreme drought

Table 6. Monthly areal extent of drought of hydrological years 1984–1985, 1987–1988, 1989–1990, 1991–1992.

Drought Year	1984–1985					1987–1988					1989–1990					1991–1992				
Month	Class 1	Class 2	Class 3	Class 4	Total	Class 1	Class 2	Class 3	Class 4	Total	Class 1	Class 2	Class 3	Class 4	Total	Class 1	Class 2	Class 3	Class 4	Total
Oct	9.8	15.6	23.7	158.6	**207.7**	0.0	0.0	0.0	0.0	**0.0**	75.2	0.0	0.0	0.0	**75.2**	81.8	0.1	0.0	0.0	**81.9**
Nov	85.0	0.0	0.0	0.0	**85.0**	0.2	0.0	0.0	0.0	**0.2**	164.9	3.0	0.0	0.0	**167.9**	163.8	0.0	0.0	0.0	**163.8**
Dec	95.5	0.0	0.0	0.0	**95.5**	66.2	0.0	0.0	0.0	**66.2**	23.0	0.0	0.0	0.0	**23.0**	0.1	0.0	22.0	183.7	**205.8**
Jan	82.0	0.1	0.0	0.0	**82.1**	76.7	9.6	0.0	0.0	**86.3**	40.1	0.0	0.0	167.6	**207.7**	197.5	10.2	0.0	0.0	**207.6**
Feb	2.4	0.0	0.0	0.0	**2.4**	0.2	0.0	0.0	0.0	**0.2**	36.1	122.4	49.3	0.0	**207.8**	53.5	118.0	24.3	11.7	**207.5**
Mar	0.3	0.0	0.0	0.0	**0.3**	0.2	0.0	0.0	0.0	**0.2**	0.0	18.0	138.3	51.5	**207.8**	36.1	33.0	134.8	0.0	**203.9**
Apr	167.1	0.1	0.0	0.0	**167.1**	127.7	0.0	0.0	0.0	**127.7**	122.3	37.2	0.0	0.1	**159.6**	0.2	0.0	0.0	0.0	**0.2**
May	79.6	8.4	0.0	38.0	**125.9**	156.8	39.4	0.0	0.0	**196.2**	1.9	0.1	0.1	0.0	**2.1**	12.5	0.0	0.0	0.0	**12.5**
Jun	87.8	4.1	40.3	72.9	**205.1**	21.8	11.7	26.2	0.0	**59.8**	161.3	0.1	0.1	0.1	**161.5**	8.5	0.0	0.0	0.0	**8.5**
Jul	90.7	38.0	0.0	0.0	**128.7**	22.5	38.0	0.0	0.0	**60.5**	39.9	0.1	0.1	0.1	**40.1**	8.4	0.0	0.0	0.0	**8.4**
Aug	114.9	0.0	0.0	0.0	**115.0**	81.9	10.2	36.1	2.5	**130.7**	0.1	0.1	0.0	0.0	**0.3**	0.2	10.2	36.2	157.2	**203.8**
Sep	63.0	8.4	38.0	14.0	**123.3**	83.7	0.0	0.0	0.0	**83.7**	77.0	0.0	0.0	0.0	**77.0**	55.8	8.3	38.7	101.3	**204.1**
Total	**878.0**	**74.6**	**102.0**	**283.6**	**1338.3**	**637.9**	**109.0**	**62.4**	**2.6**	**811.8**	**741.9**	**180.8**	**187.9**	**219.4**	**1330.0**	**618.4**	**179.8**	**256.0**	**453.9**	**1508.0**

Legend: The values are in number of pixels (each pixel = $8 \times 8\,km^2$) per drought class (the classes are in numbers as in Table 2).
Class 1 = mild, class 2 = moderate, class 3 = severe, class 4 = extreme.

Table 7. Monthly areal extent of drought of hydrological years 1992–1993, 1996–1997, 1999–2000, 2000–2001.

Drought Year	1992–1993					1996–1997					1999–2000					2000–2001				
Month	Class 1	Class 2	Class 3	Class 4	Total	Class 1	Class 2	Class 3	Class 4	Total	Class 1	Class 2	Class 3	Class 4	Total	Class 1	Class 2	Class 3	Class 4	Total
Oct	111.1	0.0	0.0	0.0	**111.2**	2.6	0.0	0.0	0.0	**2.6**	26.0	0.0	0.0	0.0	**26.0**	16.7	0.0	0.0	0.0	**16.7**
Nov	107.6	20.7	0.0	0.0	**128.3**	29.8	139.2	38.8	0.0	**207.8**	8.4	0.0	0.0	0.0	**8.4**	0.2	68.3	135.3	3.9	**207.7**
Dec	192.3	10.9	0.0	0.0	**203.2**	45.3	0.0	0.0	0.0	**45.4**	70.3	3.9	0.0	0.0	**74.2**	161.1	30.2	14.0	0.0	**205.3**
Jan	199.0	0.0	0.0	0.0	**199.0**	72.4	0.1	0.0	0.0	**72.4**	199.3	0.0	0.0	0.0	**199.3**	41.0	0.0	0.0	0.0	**41.0**
Feb	45.3	0.0	0.0	0.0	**45.3**	197.3	2.0	0.0	0.0	**199.4**	22.1	0.0	0.0	0.0	**22.1**	138.2	26.2	0.0	0.0	**164.5**
Mar	199.4	0.3	0.0	0.0	**199.7**	201.4	0.0	0.0	0.0	**201.4**	164.8	37.0	5.7	0.0	**207.4**	43.8	149.8	14.0	0.0	**207.6**
Apr	138.7	67.7	0.0	0.0	**206.4**	0.4	0.0	0.0	0.0	**0.4**	143.0	60.8	0.0	0.0	**203.7**	4.8	0.0	0.0	0.0	**4.8**
May	0.1	0.0	0.0	0.0	**0.1**	38.1	143.5	0.0	26.2	**207.8**	144.0	0.0	1.8	39.5	**185.3**	14.0	0.0	0.0	0.0	**14.0**
Jun	114.9	0.0	0.0	0.0	**114.9**	16.7	0.0	0.0	0.0	**16.7**	12.3	0.0	0.0	0.0	**12.3**	94.5	37.0	0.0	2.5	**134.0**
Jul	185.0	2.5	0.0	14.0	**201.5**	63.7	82.9	0.0	0.0	**146.6**	131.7	37.0	2.5	0.0	**171.3**	0.1	0.0	0.0	0.0	**0.1**
Aug	188.1	0.0	0.0	3.9	**192.0**	0.1	0.0	0.0	0.0	**0.1**	38.7	111.5	0.0	43.3	**193.6**	40.7	8.3	0.0	0.0	**49.1**
Sep	36.1	0.0	1.8	43.3	**81.3**	135.2	68.6	0.0	0.0	**203.8**	53.2	8.6	13.8	0.0	**75.6**	155.0	44.3	0.0	0.0	**199.3**
Total	**1517.9**	**102.1**	**1.8**	**61.2**	**1683.0**	**803.0**	**436.2**	**38.8**	**26.2**	**1304.3**	**1013.7**	**258.7**	**23.8**	**82.8**	**1379.1**	**710.1**	**364.2**	**163.4**	**6.4**	**1244.0**

Legend: The values are in number of pixels (each pixel = $8 \times 8\,km^2$) per drought class (the classes are in numbers as in Table 2).
Class 1 = mild, class 2 = moderate, class 3 = severe, class 4 = extreme.

class (class 4) for all drought years, two figures are produced: Fig. 4 for large areal extent drought and Fig. 5 for small areal extent drought, respectively. Furthermore, curve fitting is conducted for each of these figures resulting in the following polynomials: Eq. (16) for large areal extent drought and Eq. (17) for small areal extent drought, respectively, both with high coefficient of determination.

$$y = 0.4771x^3 - 9.7934x^2 + 78.221x - 36.078 \quad (R^2 = 0.9676) \tag{16}$$

$$y = 0.4868x^2 - 3.3415x + 4.78 (R^2 = 0.9618) \tag{17}$$

It is worth noticing that, for the large areal extent case (Fig. 4), drought starts during the first three months of the hydrological year, whereas, for the small areal extent case (Fig. 5), drought starts in spring (April). This finding signifies the possibility of using the fitted curves for monitoring and assessing drought in a region. Specifically, from Fig. 4 it is clear that, if at the beginning of the hydrological year and in particular the first three months (October–December), there is a sufficient number of pixels with extreme drought values of RDI (> 2.0), then this is an indication of a hydrological year with large areal extent drought with the maximum occurring during the summer. On the other hand, from Fig. 5 it is obvious that, if at the beginning of the hydrological year (October–December) the number of pixels with extreme drought values of RDI (> 2.0) is zero or negligible, then it is expected that, if drought occurs, it starts in spring with maximum again in the summer, but with small total areal extent. This finding justifies the use of the fitted curves of Figs. 4 and 5 along with the corresponding Eqs. (16) and (17), respectively, for drought prognostic assessment or early warning. By increasing the database with the inclusion of more drought episodes (years), it is expected that the fitted curves and the corresponding models can provide more reliable drought prognostic assessments and/or early warnings.

Finally, Fig. 6a is a sample annual composite maximum RDI map of Thessaly for the drought year 1984–1985. Similarly, Fig. 6b is the annual composite maximum RDI map of Thessaly for all the eight drought years. This Figure 6b shows the spatial variability of drought severity delineating also the areas of drought persistence within Thessaly.

6 Conclusions

The results show that drought episodes are very often in Thessaly (Table 5). Assessment of drought quantification for the evaluation of the remotely sensed RDI estimation is conducted through the use of four widely used and well-accepted error statistics: the efficiency coefficient, the coefficient of determination, the statistical bias and the root-mean-square error. The results (Table 3) are close to the perfect fit values for all the four error statistics, thus being considered quite satisfactory. It is clear that remote sensing has indicated some new capabilities in assessing and monitoring the spatiotemporal variability of drought episodes. Several drought features are analysed from the remotely sensed monthly RDI images: severity, duration, areal extent, onset and end time. For the severe and extreme droughts, the start usually coincides with the beginning of the hydrological year (October), whereas for moderate droughts the start is usually in spring (April), both lasting until the end of the hydrological year (September). There is also an increase in the areal extent of drought during each drought period with the maximum occurring usually in the summer. The findings also indicate that, in years of large areal extent, drought starts during the first three months of the hydrological year, whereas, in the years of small areal extent, drought starts in spring (April). This finding also signifies the possibility for first-guess predictive drought assessment.

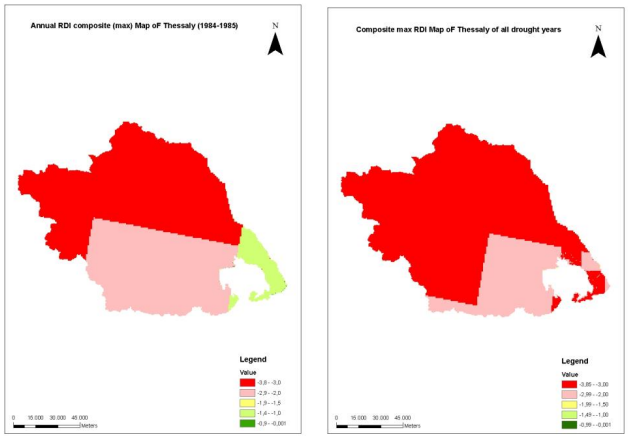

(a) Drought year 1984–1985 **(b)** All drought years.

Fig. 6. Annual remotely sensed RDI composite (max) map of Thessaly.

Acknowledgements. This research was funded by Pleiades, Smart and Hydrosense EC projects. The conventional meteorological data was provided by the National Meteorological Service of Greece. The precipitation maps were provided by the Joint Research Center (JRC) of EC, Ispra, Italy. The satellite data was provided by NOAA. Software ERDAS Imagine 8.7 was used in the analysis.

Edited by: A. M. Tarquis
Reviewed by: two anonymous referees

References

Anderson, M. C., Hain, C., Wardlow, B., Pimstein, A., Mecikalski, J. R., and Kustas, W. P.: Evaluation of drought indices based on Thermal remote sensing of evapotranspiration over the continental United States, J. Climate, 24, 2025–2044, 2011.

Blaney, H. F. and Criddle, W. D.: Determining water requirements in irrigated areas from climatological and irrigation data, USDA Soil Conservation Service, Technical Paper, No. 96, 48 pp., 1950.

Becker, F. and Li, Z. L.: Towards a local "split window" method over land surface, Int. J. Remote Sens., 3, 369–393, 1990.

Caccamo, G., Chisholm, L. A., Bradstock, R. A., and Puotinen, M. L.: Assessing the sensitivity of MODIS to monitor drought in high biomass ecosystems, Remote Sens. Environ., 115, 2626–2639, 2011.

Colwell, N. R.: Remote sensing research for agricultural applications (USA), California University, Berkeley, Space Sciences Laboratory, 1984.

Dalezios, N. R.: Objective Rainfall Evaluation in Radar Hydrology, J. Water Resour. Plan. Manag., 114, 531–546, 1988.

Dalezios, N. R., Loukas, A., Vasiliades, L., and Liakopoulos, H.: Severity-Duration-Frequency Analysis of Droughts and Wet Periods in Greece, Hydrol. Sci., 45, 751–770, 2000.

Dalezios, N. R., Bampzelis D., and Domenikiotis, C.: An integrated methodological procedure for alternative drought mitigation in Greece, European Water, 27/28, 53–73, 2009.

Du, L., Tian, Q., Huang, Y., and Liu, J: Drought monitoring based on TRMM data and its reliability validation in Shandong province, Nongye Gongcheng Xuebao/Transactions of the Chinese Society of Agricultural Engineering, 28, 121–126, 2012.

Foot, J. S.: Hazard warning in meteorology: the importance of remote sensing, in: Proceedings of IDNDR Conference on Natural Hazards and Remote Sensing, London, UK, 8–9 March, 13–16, 1993.

Heim Jr., R. R.: A Review of Twentieth- Century Drought Indices Used in the United States, B. Am. Meteorol. Soc., 83, 1149–1165, 2002.

Huang, S., Dahal, D., Young, C., Chander, G., and Liu, S.: Integration of Palmer Drought Severity Index and remote sensing data to simulate wetland water surface from 1910 to 2009 in Cottonwood Lake area, North Dakota, Remote Sens. Environ., 115, 3377–3389, 2011.

Jenkins, G. M. and Watts, D. G.: Spectral analysis and its applications, Holden-Day, San Francisco, 525 pp., 1968.

Kanellou, E., Domenikiotis, C., Tsiros, E., and Dalezios, N. R.: Satellite-based Drought Estimation in Thessaly, European Water, 23/24, 111–122, 2009.

Kanellou, E., Spyropoulos, N., and Dalezios, N. R.: Geoinformatic Intelligence Methodologies for Drought Spatiotemporal Variability in Greece, Water Resour. Manage., 26, 1089–1106, 2011.

Keyantash, J. and Dracup, J. A.: The Quantification of Drought: An Evaluation of Drought Indices, B. Am. Meteorol. Soc., 83/8, 1167–1180, 2002.

Loukas A., Vasiliades, L., and Dalezios, N. R.: Hydroclimatic variability of regional droughts in Greece using the Palmer Moisture Anomaly Index, Nordic Hydrol., 33, 425–442, 2002.

McVicar, T. R. and Jupp, D. L. B.: The Current and Potential Operational Uses of Remote Sensing to Aid Decisions on Drought Exceptional Circumstances in Australia: a Review, Agr. Systems, 57, 399–468, 1998.

Mishra, A. K. and Singh, V. P.: Drought modeling – A review, Rev. J. Hydrol., 403, 157–175, 2011.

Nash, J. E. and Sutcliffe, J. V.: River flow forecasting through conceptual models, Part-1: A discussion of principles, J. Hydrol., 10, 282–290, 1970.

Palmer, W. C.: Meteorological drought. Research Paper No. 45, US Department of Commerce, Weather Bureau, Washington, DC, 58 pp., 1965.

Peled, E., Dutra, E., Viterbo, P., and Angert, A.: Technical Note: Comparing and ranking soil drought indices performance over Europe, through remote-sensing of vegetation, Hydrol. Earth Syst. Sci., 14, 271–277, doi:10.5194/hess-14-271-2010, 2010.

Percival, D. B. and Walden, A. T.: Spectral analysis for physical applications-multitaper and conventional univariate techniques, Cambridge University Press, New York, 612 pp., 1993.

Piechota, T. C. and Dracup, J. A.: Drought and Regional Hydrology Variation in the United States: associations with the El Nino-Southern Oscillation Water Resour. Res., 32, 1359–1373, 1996.

Rhee, J., Im, J., and Carbone, G. J.: Monitoring agricultural drought for arid and humid regions using multi-sensor remote sensing data, Remote Sens. Environ., 114, 2875–2887, 2010.

Steinemann, A., Hayes, M. J., and Cavalcanti, L.: Drought indicators and triggers, in: Drought and Water Crises, Science Technology and Management Issues, edited by: Wilhite, D., Marcer Dekker Publ., 71–90, 2005.

Thenkabail, P. S., Gamage, M. S. D. N., and Smakhtin, V. U.: The Use of Remote Sensing Data for Drought Assessment and Monitoring in Southwest Asia, Research Report, International Water Management Institute, 85, 1–25, 2004.

Tsakiris, G. and Vangelis, H.: Establishing a Drought Index Incorporating Evapotraspiration, European Water, 9/10, 3–11, 2005.

Tsakiris, G., Pangalou D., and Vangelis, H.: Regional drought assessment based on the Reconnaissance Drought Index (RDI), Water Resour. Manage., 21, 821–833, 2007.

Van de Griend, A. A. and Owe, M.: On the relationship between thermal emissivity and the normalized difference vegetation index for natural surfaces, Int. J. Remote Sens., 14, 1119–1137, 1993.

Williams, J. B: Direct reception of satellite data for in-country warning, monitoring and mitigation of natural disasters in the developing world: the LARST approach, Hazard warning in meteorology: the importance of remote sensing, in: Proceedings of IDNDR Conference on Natural Hazards and Remote Sensing, London, UK, 8–9 March, 22–25, 1993.

Zhou, L., Zhang, J., Wu, J., Zhao, L., Liu, M., Lü, A., and Wu, Z.: Comparison of remotely sensed and meteorological data-derived drought indices in mid-eastern China, Int. J. Remote Sens., 33, 1755–1779, 2012.